

REPORT

Early stage of cytomegalovirus infection suppresses host microRNA expression regulation in human fibroblasts

Anton A. Buzdin^{a,b,c}, Alina V. Artcibasova^{a,d}, Natalya F. Fedorova^e, Maria V. Suntsova^{a,b}, Andrew V. Garazha^{a,f}, Maxim I. Sorokin^g, Daria Allina^{f,g}, Mikhail Shalatonin^h, Nikolay M. Borisov^{c,g}, Alex A. Zhavoronkov^{a,d}, Igor Kovalchukⁱ, Olga Kovalchukⁱ, and Alla A. Kushch^e

^aLaboratory of Bioinformatics, D. Rogachyov Federal Research Center of Pediatric Hematology, Oncology and Immunology, Moscow, Russia; ^bGroup for Genomic Regulation of Cell Signaling Systems, Shemyakin-Ovchinnikov Institute of Bioorganic Chemistry, Moscow, Russia; ^cNational Research Centre "Kurchatov Institute", Centre for Convergence of Nano-, Bio-, Information and Cognitive Sciences and Technologies, Moscow, Russia; ^dPathway Pharmaceuticals, Wan Chai, Hong Kong, Hong Kong SAR; ^eN.F. Gamaleya Federal Research Centre for Epidemiology and Microbiology of the Ministry of Health of the Russian Federation, Moscow, Russia; ^fMoscow Institute of Physics and Technology, Dolgoprudny, Moscow region, Russia; ^gFirst Oncology Research and Advisory Center, Moscow, Russia; ^hThe Morozov Children's City Hospital, Moscow, Russia; ⁱDepartment of Biological Sciences, University of Lethbridge, Lethbridge, AB, Canada

ABSTRACT

Responses to human cytomegalovirus (HCMV) infection are largely individual and cell type specific. We investigated molecular profiles in 2 primary cell cultures of human fibroblasts, which are highly or marginally sensitive to HCMV infection, respectively. We screened expression of genes and microRNAs (miRs) at the early (3 hours) stage of infection. To assess molecular pathway activation profiles, we applied bioinformatic algorithms OncoFinder and MiRImpact. In both cell types, pathway regulation properties at mRNA and miR levels were markedly different. Surprisingly, in the infected highly sensitive cells, we observed a "freeze" of miR expression profiles compared to uninfected controls. Our results evidence that in the sensitive cells, HCMV blocks intracellular regulation of microRNA expression already at the earliest stage of infection. These data suggest somewhat new functions for HCMV products and demonstrate dependence of miR expression arrest on the host-encoded factors.

ARTICLE HISTORY

Received 8 August 2016
Revised 12 September 2016
Accepted 21 September 2016

KEYWORDS

Cytomegalovirus infection; gene transcription; human fibroblasts; intracellular signaling pathway regulation; microRNA; total miRNAome

Introduction

The infections by human cytomegalovirus (HCMV; also known as CMV and HHV-5) can be symptomless and latent throughout life for the majority of the affected immunocompetent individuals. However, first contact with the infection, reinfection, or reactivation of HCMV in persons with underdeveloped or compromised immune system, can lead to a severe, sometimes fatal disease.^{1–2} For example, HCMV is the leading viral cause of congenital birth defects.³ In addition, HCMV infection may act as an oncogenic transformation cofactor in various cell types.⁴ HCMV infection starts when viral proteins bind to the cell surface, and the virus enters the cell and causes reprogramming of the intracellular processes.⁵ Immediate early genes (0–4 hours after infection) participate in the regulation of transcription, followed by early genes (4–48 hours after infection) which are involved in viral DNA replication and further transcriptional regulation.⁶ Late genes are expressed during the remainder of infection up to viral egress and typically code for structural proteins.

Early stages determine the fate of the infection process, for example, whether it will be lytic or latent.⁵ At the early time of HCMV infection, 2 layers of viral gene regulation are thought


critical according to classical model: *i*) *IE* (immediate early) gene regulation through the interaction of cellular factors with the major *IE* promoter and enhancer, and *ii*) activation of early genes by *IE* proteins.⁵ A plethora of data is available today on the involvement of certain viral and host cellular genes in the course of infection.⁷ However, a comprehensive understanding of infection processes at the early stages, including changes in transcriptomes and microRNA profiles and interactions between them, is still missing.

MicroRNAs (miRs) are 19 to 24 nucleotides long non-coding RNAs that regulate the expression of target mRNA molecules, both at the transcriptional and translational levels.^{8–9} They influence all major physiological processes, such as development, growth, differentiation, immune reaction, and adaptation to stress.^{10–11} Specific miR programs are activated in normal physiological or pathological processes, including infections.^{12–13}

In this study, we used a combination of experimental and bioinformatic approaches to elucidate response of human cells to HCMV at the early stage of infection (3 hours after inoculation). We profiled the expression of miRs and of protein coding genes for the 2 untransformed normal human fibroblast cell

CONTACT Anton A. Buzdin  bu3din@mail.ru  Shemyakin-Ovchinnikov Institute of Bioorganic Chemistry, Miklukho-Maklaya 16/10, Moscow 117997, Russia.

Color versions of one or more of the figures in the article can be found online at www.tandfonline.com/kccy.

 Supplemental data for this article can be accessed on the publisher's website.

lines HELF-977 and HAF-1608, which were obtained from embryonic and adult tissues, accordingly, and had markedly different sensitivity to HCMV.

In this study, we generated a list of differentially expressed genes and miRs in response to HCMV infection for these 2 cell cultures. To further analyze the expression data, we applied a bioinformatic algorithm termed OncoFinder for the characterization of molecular pathway activation. OncoFinder allows analyzing quantitatively and qualitatively the activity of intracellular molecular pathways based on high throughput gene expression profiles. For each investigated sample, it performs a case-control pairwise comparison and calculates Pathway Activation Strength (PAS), a value that serves as a qualitative measure of a pathway activation. Negative and positive PAS values correspond, respectively, to inhibited or activated states of the corresponding molecular pathways.¹⁴ This method was reported to provide output data with significantly reduced level of noise introduced by the experimental platforms.¹⁵ The version of the OncoFinder database used in this study features 2 725 gene products and 271 signaling pathways. To date, OncoFinder algorithm has been applied for various objects, including induced stem cells,¹⁶ asthma,¹⁷ leukemia,¹⁸ and solid tumors,¹⁹⁻²⁰ Hutchinson-Gilford and age-related macular degeneration diseases.²¹⁻²²

On the other hand, to assess the overall effects of miR expression profiles during HCMV infection, we applied another recent method, termed *MiRImpact*,²³ which utilizes OncoFinder rationale for pathway activity calculations, but with the distinctions that (i) it processes concentrations of miRs that are known regulators of genes participating in molecular pathways, and (ii) miRs are considered as negative regulators of their target molecules. *MiRImpact* operates with 2 types of databases: for molecular targets of miRs and for gene products participating in molecular pathways. Here, we used the *MiRImpact* method to monitor PAS regulation at miR level (miPAS) in the infected cells.

We observed that in both cell lines, pathway regulation properties at mRNA and miR levels were markedly different. Initial pathway regulation at the miR level was orthogonal to that based on mRNA concentrations. We found that in highly sensitive cells, infection dramatically altered both mRNA and miR expression already 3 hours after infection. This was not the case for marginally sensitive cells, which displayed expression patterns similar to uninfected control population. Surprisingly, in the infected highly sensitive cells, we observed a “freeze” of miR expression patterns compared to uninfected controls. Our results suggest that HCMV infection can block intracellular regulation of miR expression already at the earliest stage of infection. These data suggest somewhat new functions for the HCMV/host cells molecular interplay.

Materials and methods

Cell culture

We examined 2 human fibroblasts cell lines: normal embryonic lung fibroblasts (line HELF- 977) and normal fibroblasts from the skin of an adult donor (line HAF-1608, on the 15th passage after establishment of the cell line). Both cell lines were obtained from the collection of cell cultures at the N.F.

Gamaleya Federal Research Centre for Epidemiology and Microbiology (Moscow, Russia). The cells were grown in Dulbecco's modified Eagle's medium, DMEM, (Gibco, USA) supplemented with 10% fetal bovine serum, FBS, (HyClone, USA), 2 mM L-glutamine and 50 ug/ml gentamicin at 37°C in 5% CO₂. The cells were grown by regular passaging until confluence was reached. To obtain cells in the G₀ phase of the cell cycle, the cells were held in DMEM with 0.2% FBS for 48 hours.

HCMV infection

The human cytomegalovirus (HCMV) strain AD-169 was obtained from the State Collection of Viruses at the N.F. Gamaleya Federal Research Centre for Epidemiology and Microbiology (Moscow, Russia). Cells HELF- 977 and HAF-1608 synchronized in the G₀ phase were infected with HCMV at a multiplicity of infection of 3, or mock infected. Viral inoculum was added to the cells and allowed to adsorb for 60 min at 37°C in 5% CO₂. Next, the viral inoculum was replaced with fresh medium. Three hours after infection, the cells were collected and aliquots were frozen in liquid nitrogen. For each cell line, we examined 3 samples: (i) the pre-analysis norm representing cells before infection, (ii) infected cells 3 hours after medium replacement (3H AI), and (iii) mock-infected cells 3 hours after medium replacement (3H WI). For the analysis of CMV AD-169 growth characteristics in HELF- 977 and HAF-1608 cells, the virus-containing medium was collected when cytopathic effects were >90%. Supernatants were clarified of cell debris by centrifugation at 1500g for 10 min at 4°C and were stored at -70°C until use. Virus titers were determined at 1, 2, 3 and 4 days after infection by plaque-forming unit (PFU) titration in human fibroblasts according to standard procedures.

Immunocytochemical analysis

Cells grown on coverslips were fixed for 20 min at -20°C in cold methanol. For staining cells were incubated at 37°C for 60 min with 50 µl of anti-CMV antibodies to IE1/2 (Abcam, UK, ab 53495), to pp65 (Abcam, ab 53489) and to gB (Abcam, ab 54023) diluted 1:250 in PBS containing 1% BSA. After three washes with PBS cells were incubated with 50 µl of peroxidase-labeled rabbit anti-mouse immunoglobulin G (Dako, Denmark, P0260) diluted 1:100 in PBS containing 1% BSA and after washing in PBS were incubated with 50 µl of substrate consisting of 0,5 mg/ml of diaminobenzidine and 0,5% H₂O₂ in 1M Tris (pH8) for 15 min at RT. After washing in PBS cells were analyzed under a microscope Zeiss AXIO Scope.

Microarray profiling of gene expression

Total RNA was extracted from the HELF- 977 and HAF-1608 cells using TRIzol (Life Technologies, USA) and then reverse-transcribed to cDNA and cRNA using the Ambion TotalPrep cRNA Amplification Kit (Invitrogen, USA). Also, cRNA was quantified using a NanoDrop ND-1000 Spectrophotometer (NanoDrop Technologies, USA) and adjusted to a concentration of 150 ng/mL. Then, 750 ng of each library was hybridized onto the bead arrays using Illumina HumanHT-12v4 Expression Bead-Chip (Illumina, USA). It has > 25,000 annotated human genes

and > 48,000 probes derived from the NCBI RefSeq (Build 36.2, Rel 22) and UniGene (Build 199) databases. The microarray hybridization experiments were done at Genoalytica (Moscow, Russia) using the Illumina HumanHT-12v4 Expression BeadChip (Illumina, USA). Gene expression data were deposited in the Gene Expression Omnibus database (<http://www.ncbi.nlm.nih.gov/geo/>) under accession number GSE75366.

Sequencing of short RNA fraction

Short RNA fractions from total RNA extracts were cloned as previously described.²⁴⁻²⁵ Non-coding RNAs within a 19–33 nt window were isolated from 12% polyacrylamide gels. Additionally, 3'- and 5'-linkers were ligated, and products were reverse-transcribed using Superscript III (Invitrogen). Following PCR amplification, the libraries were sequenced using the Illumina GAIIx platform in accordance with Illumina protocols (Illumina, USA). Primary RNA sequencing data were deposited in the Gene Expression Omnibus database (<http://www.ncbi.nlm.nih.gov/geo/>) and the Sequence Read Archive database (<https://www.ncbi.nlm.nih.gov/Traces/sra/>) and are available under accession numbers GSE75305.

Primary analysis of small RNA reads

After FASTQ to FASTA conversion, the adapter sequence (5'-TGGAATTCTCGGGTGCCAAGG-3') was clipped from the 3'-end of raw reads, and reads shorter than 16 nt were discarded. The remaining sequences were mapped to the miRBase reference using the short-read aligner Bowtie,²⁶ and up to 2 mismatches were allowed. The sequences that failed to map to the genome were mapped against the artificially introduced sequences. The multiplicity count of mapped sequences was normalized to the total number of reads that mapped to the genome. Aligned reads were attributed to known microRNAs using processing with SAMTools.²⁷

Molecular pathways

The signaling pathways knowledge base (developed by SABiosciences) (<http://www.sabiosciences.com/pathwaycentral.php>) was used to determine the structures of intracellular pathways, which were used for OncoFinder, as described previously.^{15,18}

Functional annotation of gene expression data

For the functional annotation of gene expression data at the molecular pathway level, we applied the OncoFinder algorithm, recently published by Buzdin et al.¹⁵ It operates with a calculation of PAS, a value which serves as a qualitative measure of a molecular pathway activation. The formula for PAS calculation accounts for gene expression data and for information on the protein interactions in a pathway, namely, the individual protein activator or repressor roles in a pathway.

For pathway p , $PAS_p = \sum_n ARR_{np} \cdot \log(CNR_n)$, where n is an individual gene product belonging to pathway p . The relative role of a gene product in signal transduction is reflected by a discrete

flag *activator/repressor role* (ARR), which equals 1 for an activator gene product, and -1 for a repressor and shows intermediate values of -0.5 , 0.5 , and 0 for the gene products that have repressor, activator, or unknown roles, respectively. The CNR_n value (*case-to-normal ratio*) is the ratio of the expression level of a gene n in the sample under investigation to the average expression level in the reference sampling. The positive value of PAS indicates abnormal activation of a signaling pathway, and the negative value indicates its repression. Here, the case-to-normal ratio, CNR_n , is the ratio of expression levels for a gene n in the sample under investigation to the same average value for the control group of samples. In addition, for each CNR_n value, we applied multiplication to a Boolean flag of *BTF* (beyond tolerance interval flag), which equals 1 when the CNR_n value passed, and to 0 when the CNR_n value did not pass both or either one of the 2 criteria of significantly differential expression: first, the expression level for the sample must fit outside of the tolerance interval for norms, with $p < 0.05$, and second, the value of CNR_n must differ from 1 by at least 1.5-fold.

MiRImpact algorithm

The MiRImpact algorithm utilizes next-generation sequencing data on non-coding RNAs, mapped to a specific miR target database, and calculates miR pathway activation strength (*miPAS*). The formula for *miPAS* calculation includes miR expression data and the information on the mRNA targets for each particular miR. For a certain pathway p ,

$$miPAS_p = \sum_n (-ARR_{np}) \cdot \sum_k \log(miCNR_{nk}).$$

Summation is done for all the gene products participating in a pathway p . The role of a gene product in a pathway p is reflected by a discrete flag *activator/repressor role* (ARR_{np}), which equals 1 for an activator gene product, -1 for a repressor, and intermediate values -0.5 , 0.5 , and 0 for the gene products that have repressor, activator, or unknown roles, respectively. Inner summation is done over all the miRs affecting pathway p . The $miCNR_k$ value (microRNA case-to-normal ratio) is the ratio of the expression level of microRNA k in the sample under investigation to the average expression level in the group of normal samples. The positive value of $miPAS_p$ indicates abnormal activation of a signaling pathway by microRNA profiles, and the negative value indicates its repression.

MiR target databases

We collected, analyzed, and preprocessed data from experimentally validated microRNA target databases miRTarBase²⁸ and Diana TarBase²⁹ to include the data in the MiRImpact database.

OncoFinder and MiRImpact settings

To analyze the patterns of differential pathway activation, we used 2 methods: OncoFinder¹⁵ and MiRImpact²³ and the corresponding software. Prior to analysis, quantile normalization was applied to microarray gene expression data. AI and WI samples were

treated as the “case” samples. Pre-experimental normal samples were used as the “norm” samples. The analysis was done separately for HCMV infection in HS and LS cell cultures.

Differential analysis of gene expression data

Upregulated and Downregulated Pathways. We used 3 parameters to select upregulated and downregulated pathways for both cultures for PAS and miPAS values. First, *difference* is the absolute value of a difference between PAS or miPAS values for AI and WI biosamples ($|AI - WI|$). Second, *positive* is the logical value that shows if the sign of a difference (AI - WI) is positive (TRUE for upregulated and FALSE for downregulated pathways). This denotes what PAS or miPAS value increased or decreased in the infected compared to the control sample. Third, to identify differential pathways, we used a *difference cut-off* of 2 (roughly corresponding to the apparently observed 10% of the smallest difference between maximum and minimum PAS value in a sample). The molecular pathways for which the *difference* was lower than the cut-off value were referred to as *unchanged*.

Heat maps. To generate heat maps, we used the function *heatmaps.2* (R package *gplots*) for both types of comparison: HS versus LS cell cultures and normal vs. infected samples. The color palette was symmetrical relatively to zero. Dependencies PAS versus miPAS were calculated using validated miR target databases, the miRTarBase²⁸ and Diana TarBase,²⁹ and plotted using function *R plot*.

Results

Biosamples and HCMV infection

We examined 2 untransformed normal human fibroblast cell lines, HELF-977 and HAF-1608. Both were taken on the 15th passage after establishing the respective cell lines. The proliferative activities of HELF-977 and HAF-1608 cells differed substantially: the rate of [³H] thymidine incorporation in the nuclear DNA reflecting activity of DNA synthesis and the growth rate were significantly greater in fetal line HELF-977 than in the HAF-1608 cells isolated from the skin of an adult donor. The time of full monolayer formation was 2 to 3 days for HS HELF-977 cells and 6 to 7 days for LS HAF-1608 cells at the same initial concentrations.

In order to minimize the effects of the different stages of the cell cycle on the infection efficiencies, the cells were synchronized in the G₀ phase of the cell cycle and then infected with the human cytomegalovirus (HCMV) strain AD-169 at a multiplicity of infection of 3. In parallel, a fraction of each cell culture was mock infected with the same buffer solution. Viral inoculum was added to the cells and allowed to adsorb for 1 hour and then removed and replaced with fresh medium. Up to 72 hours after infection, the HELF-977 cells expressed immediately early IE72 and early pp65 HCMV proteins at significantly higher levels than in the HAF-1608 cells (Figs. 1A, 2A, B). Furthermore, a late gB HCMV protein was detected in HELF-977 cells as early as 24 hours after infection, but in HAF-1608 fibroblasts – only 48 hours after infection (Figs. 1B,

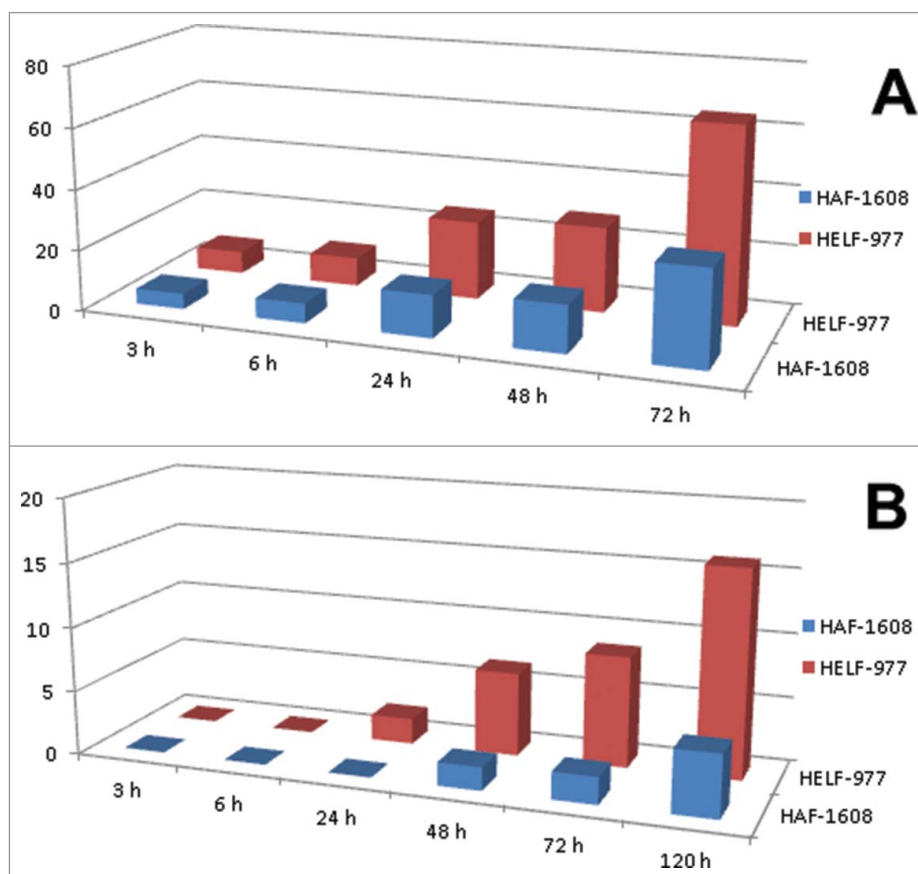


Figure 1. Detection of HCMV proteins in infected human fibroblasts. Infected cells grown on coverslips were fixed and stained with the antibodies against early pp65 HCMV protein (A) and late gB HCMV protein (B). Abscissa – time after infection, hours; ordinate – proportion of stained cells, %.

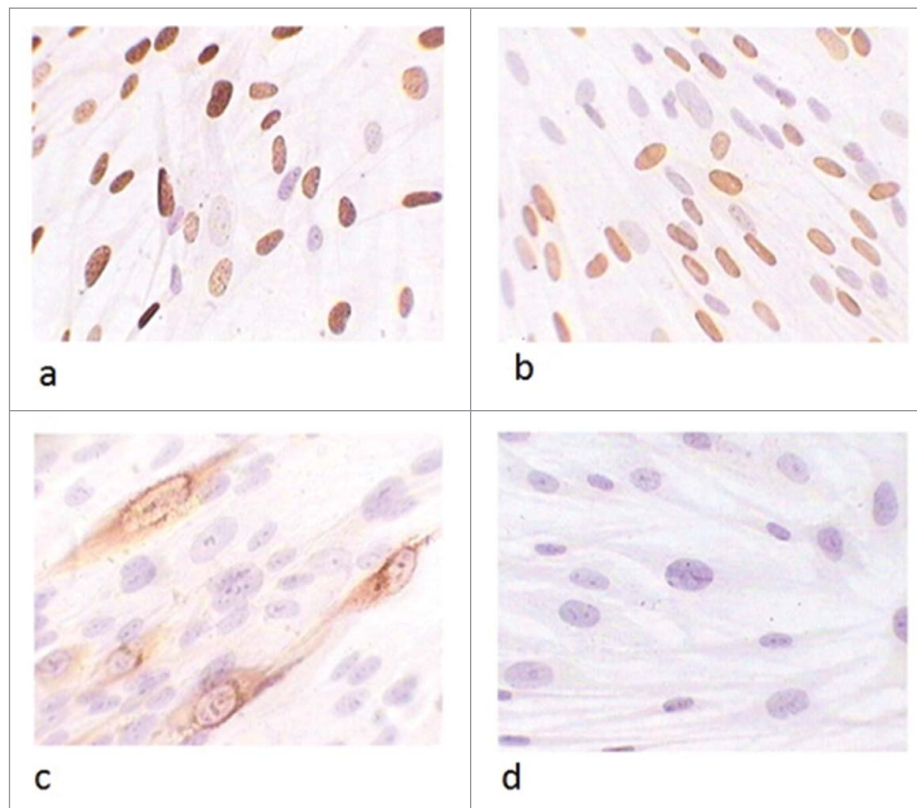


Figure 2. Immunocytochemical detection of HCMV proteins in HELF-977 cells 72 hours after infection. Panels represent staining with the antibodies against immediately early IEp72 protein (A), early pp65 protein (B); late gB protein (C). Noninfected (control) cells stained with the antibodies against immediately early IEp72 protein are shown on panel D.

2C). HCMV-specific changes in the size and shape of cells were seen in HELF-977 within 3 days after infection (Fig. 2C) and in HAF-1608 - within 7 days after infection. Infectious activity of HCMV produced was detected by titration and was ~12 times bigger in HELF-977 than in HAF-1608 (Fig. 3). These data allowed to characterize HELF-977 cells as highly sensitive (HS) and HAF-1608 - as low sensitive (LS) to HCMV infection.

Three hours after infection, the cells were collected and aliquots were taken for RNA isolation and expression profiling. For each cell line, we examined 3 samples: (i) the pre-analysis norm representing cells before infection, (ii) infected cells 3 hours after infection (3H AI), and (iii) mock-infected cells 3 hours after mock infection (3H WI). For the analysis, we chose the early stage of HCMV infection because the first few hours after infection play a key role in reshaping the intracellular molecular landscape, which determines the fate of an infected cell.³⁰

Profiling of RNA expression and activation of molecular pathways

We used deep sequencing to establish microRNA expression profiles and microarray hybridization to interrogate transcription of protein coding genes. The data on mRNA and miR expression were deposited at the Gene Expression Omnibus database, with the accession numbers GSE75366 and GSE75305, respectively.

RNA expression data were further processed to establish the activation features of intracellular molecular pathways. We

analyzed gene expression (the mRNA level) using the OncoFinder algorithm and the corresponding software.¹⁵ A total of 271 intracellular signaling pathways were assayed (Supplementary dataset 1). To assess pathway regulation at the microRNA (miR) level, we used the MiRImpact method recently developed in our consortium.²³ The algorithm MiRImpact was built to characterize the effects, provoked by the changes in overall miR

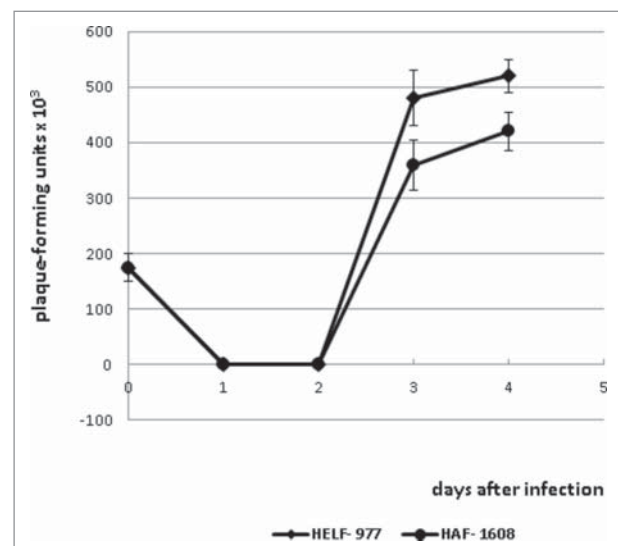


Figure 3. Curve of HCMV titers produced in HELF-977 and HAF-1608 fibroblasts. Virus titers were determined at 1, 2, 3 and 4 days after infection by plaque-forming unit (PFU) titration and presented as PFUx10³.

Table 1. Statistics of the validated miR target databases, based on the data collected from miRTarBase, Diana TarBase and OncoFinder pathway databases.

Characteristics	miRTarBase	Diana TarBase
Number of microRNAs	596	183
Number of target genes	12103	3006
Number of target genes overlapping with OncoFinder pathway database	1968	497

concentrations. It quantifies their impact on the activity of intracellular molecular pathways. MiRImpact was developed on the basis of a rationale previously published for the OncoFinder algorithm.¹⁵ Similarly to the approach used in OncoFinder, the approach used in the MiRImpact takes into consideration a differential expression for each miR calculated relative to control biosamples. To calculate the miR-based pathway activation strength (miPAS) value, all miRs targeting gene products participating in a pathway are considered, with the assumption that they specifically inhibit their targets. In agreement with OncoFinder, a positive value of miPAS indicates activation of a pathway and vice versa. Zero value indicates that pathway is similarly activated to the normalization control transcriptome or group of transcriptomes. In our study, we took the normalization controls representing cells before infection for both cell lines.

To perform miR analysis, we used 2 alternative knowledge bases of miRs and their experimentally validated targets: the miRTarBase²⁸ and Diana TarBase²⁹ (Supplementary data set 2). Target specificities of the enclosing miRs cover, respectively, 72% and 18% of the gene products listed in the OncoFinder database (Table 1). Both databases include information on more than 50,000 molecular interactions of miRs with target mRNA molecules. This information is manually curated by the publishers based on the available literature.^{28,31} For all calculations, AI and WI expression profiles were normalized on the data obtained for the initial pre-infection cells. For all the samples, we observed statistically significant correlations between the miPAS scores, which were calculated using both miRTarBase and Diana TarBase databases (Fig. S1). Specifically, samples without infection (WI), especially for the HS culture, demonstrate linear relationship. Samples after infection (AI) generally support this trend, but lower miPAS value ranges lead to higher levels of noise Fig. S1). This suggests that both databases provide an adequate basement for the pathway regulation analysis. However, the miRTarBase is far more complete in terms of the greater number of miR targets included, and in this study, we focused on the results obtained with the miRTarBase data.

HCMV infection-linked changes in gene and molecular pathway activity

We obtained overall pathway activation profiles, using OncoFinder for mRNA regulation levels (Supplementary dataset 1) and MiRImpact for miR regulation levels (Supplementary data set 2). Heat maps were built to visualize differences in pathway activation between the samples (Supplementary dataset 3). We established large-scale profiles of intracellular signaling pathway activation associated with the HCMV infection. These

profiles were markedly different for the fibroblasts with high and low sensitivity to infection at both levels of RNA regulation. Similarly to the previously published data for bladder cancer,²³ we observed that the intracellular pathway regulation at the miR level differs greatly from that at the mRNA level, thus showing orthogonal dependencies for the extent of pathway activation (Fig. 4). In general, we observed that in the HS cells, the proportion of upregulated pathways at the PAS level was significantly higher compared to the LS fibroblasts for both infected and non-infected conditions (Fig. 5; Supplementary data set 4): 39% vs. 20% of upregulated pathways in HS and LS cells, respectively. Similarly, the proportion of downregulated pathways in HS cells also increased compared to the LS cells: 30% versus 10% of downregulated pathways in HS and LS cells, respectively. Consistently, the number of unaffected pathways was much higher in the LS culture: 57% vs. 29% in the HS cells.

When looking at the non-infected cells, at the miPAS level the number of upregulated pathways was even bigger than at the PAS level: 65% versus 39% for the HS cells and 38% vs. 20% for the LS cells for the miPAS and PAS scoring, respectively (Fig. 5, Supplementary dataset 4). For the LS cells, we observed the highest proportion of unchanged (intact) pathways linked with the HCMV infection. In particular, the intact group at both mRNA and miR levels formed 26.5% of the pathways, and the group with intact regulation at the mRNA level and upregulation at the miR level formed 25.2% of the pathways (Table 2).

In contrast, for the HS cells, the biggest groups were pathways upregulated at both the mRNA and miR levels (29.3% of the pathways) and pathways downregulated at the mRNA level and upregulated at the miR level (21.7% of the pathways). Notably, upregulation at both mRNA and miR levels appeared to be sixfold higher in the HS as compared to LS cells. The LS cells, in turn, had a sevenfold greater proportion of the intact pathways than the HS cells (Table 2, Supplementary data set 4).

At the mRNA level, 19 molecular pathways were upregulated and 12 were downregulated in both the HS and the LS cells during HCMV infection. Similarly, at the level of miR regulation in the HS and the LS cells, 57 molecular pathways were upregulated and 9 were downregulated, respectively, during HCMV infection (Supplementary data set 4). Finally, 8 pathways showed identical trends in both the HS and the LS cells, at both the PAS and miPAS levels of regulation. Of these, the EGFR1 and ErbB family pathways were upregulated, while others were downregulated (Supplementary data set 4).

HCMV infection-specific suppression of miR regulation

We also detected several trends characterizing large-scale behaviors of the infected vs non-infected HS and LS cells at the molecular level. First, for the time-control (WI) HS cells, overall sets of RNA regulation features showed significantly greater levels of variation compared to the LS cells: at the mRNA level (Fig. 6A, B), at the miR level (Fig. 6C, D) and at the signaling pathway regulation levels (PAS and miPAS; Fig. 4A, B). Since case-to-normal ratio (CNR), PAS and miPAS values were obtained when comparing gene expression with the pre-infection controls, this suggests that the HS cells are prone to change their molecular landscapes more rapidly than the LS cells

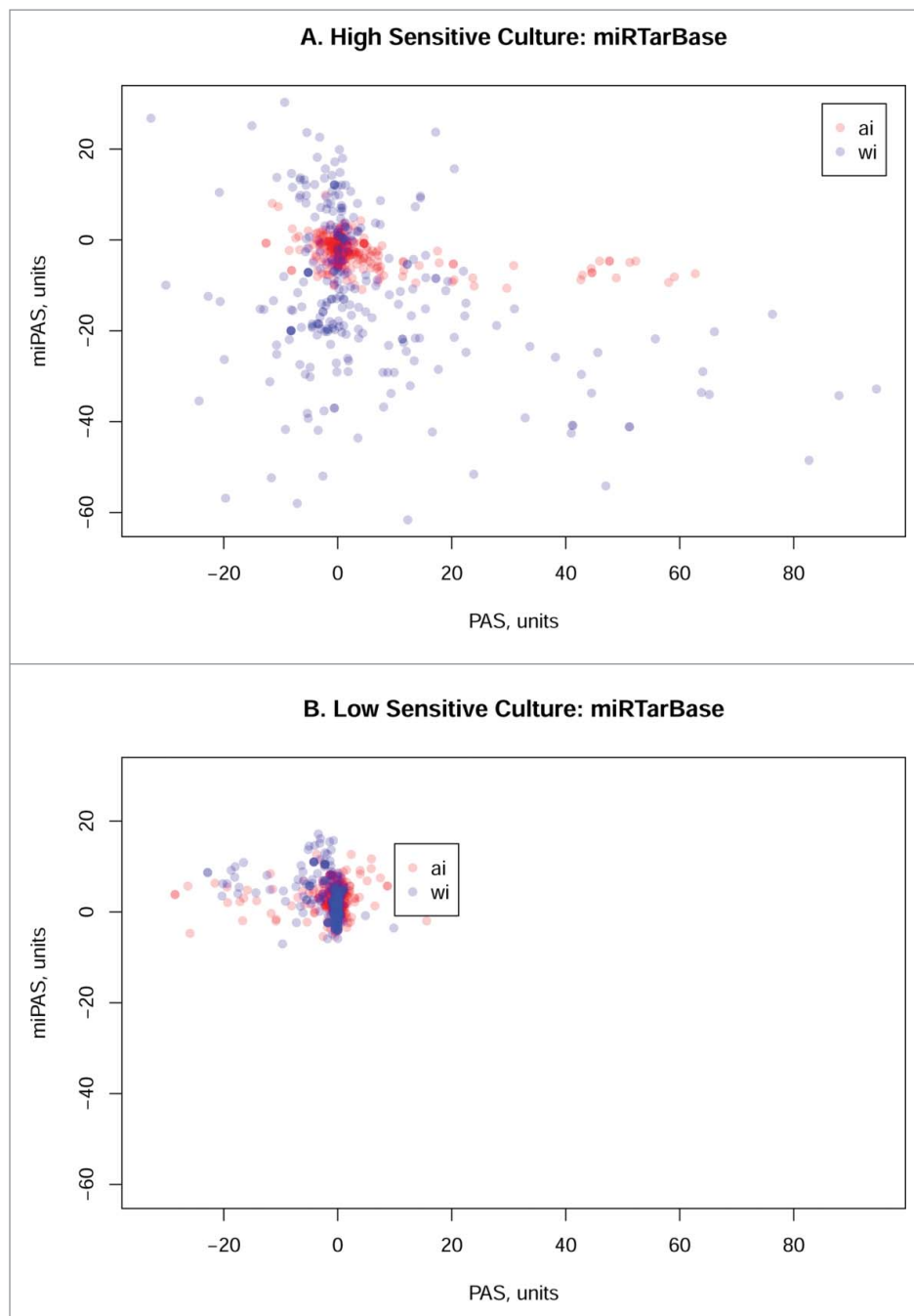


Figure 4. Dependencies between Pathway Activation Strength (PAS) and microRNA Pathway Activation Strength (miPAS). MiPAS data were calculated using miRTarBase database. Each dot represents one molecular pathway, for which PAS and miPAS values were calculated. Blue dots are given for the samples without HCMV infection, red dots – for the samples after infection. All PAS and miPAS values were calculated against pre-infection controls. A, comparison for the HS cells; B, comparison for the LS cells.

even in the non-infected conditions. The same was also true for the infected HS cells, but only for the regulation at the mRNA and PAS levels (Figs. 4A, 6A).

Second, for the infected HS cells, we observed a dramatically lower impact of miR regulation of the molecular pathways, as reflected by close-to-zero clouds of CNR (Fig. 6C) and miPAS (Fig. 4B) values compared to the mock-infected controls. It means that the infected HS cells demonstrate little difference from the pre-infection controls in their miR expression profile. This is evidenced by the respective distribution curves with approximately 3-fold lower dispersion for the AI cells compared to WI cells for the miR CNRs (Fig. 7), and about 5-fold

lower – for the miPAS values (Supplementary dataset 5). Notably, no significant bias in distribution trends could be seen for the LS cells, and, at the levels of mRNA and PAS – in both cell types (Supplementary data set 5). Such an effect shows conservation of miR expression landscape in the highly sensitive fibroblasts at the moment of HCMV invasion and further, at least up to 3 hours after infection. We propose that this may be due to a previously unknown property of HCMV proteins to suppress intracellular defensive mechanisms related to miR expression. This finding evidences that at the early stage of HCMV infection, the miR regulation in the host cells is significantly suppressed. Interestingly, this suppression was not seen

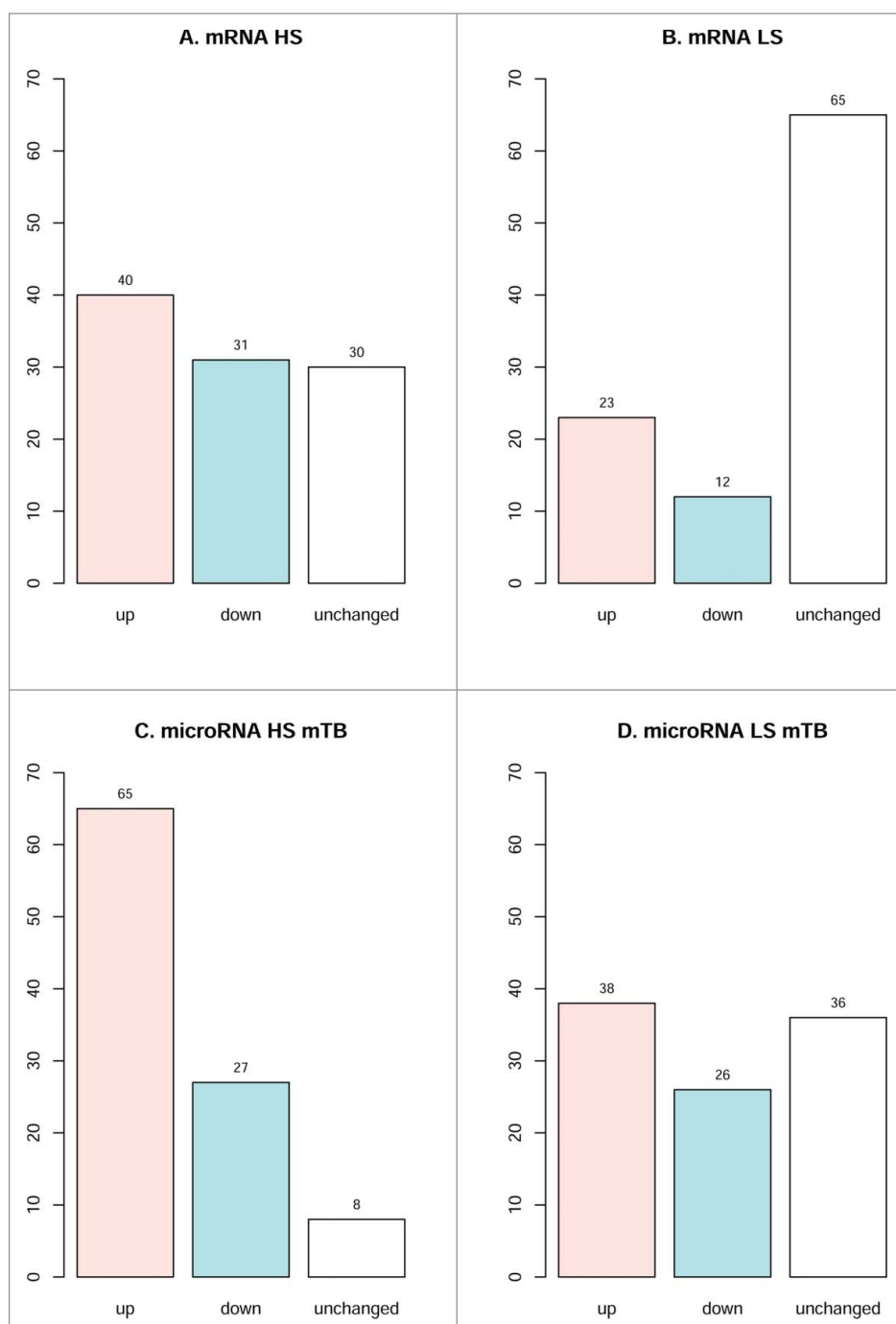


Figure 5. Statistics of the affected molecular pathways in infected fibroblasts. “Up” and “down” groups for each type cells include pathways showing difference between PAS or miPAS values bigger than predefined threshold value. MiPAS data were calculated using miRTarBase database. All PAS and miPAS values were calculated against pre-infection controls. A, mRNA-based PAS data calculated for the HS cells. B, mRNA-based PAS data calculated for the LS cells. C, miR-based miPAS data calculated for the HS cells. D, miR-based miPAS data calculated for the LS cells.

for the LS cells (Figs. 6 and 7), which may suggest its importance for the progression of the HCMV infection.

Discussion

Information about the cellular mechanisms involved in the early regulation of HCMV infection on the microRNA and mRNA level is not sufficient. The data available usually refer to the later stages of infection (24–72 h), corresponding to the synthesis of viral DNA and HCMV structural proteins. Thus, Browne et al. have shown that during a 48-hour time course

after the infection of human diploid fibroblasts, 1,425 cellular mRNAs can be upregulated or downregulated by threefold or greater.³² Analysis of primary pathways allowed to identify HCMV products interacting with the cellular machinery. Roy and Arav-Boger,³³ in a review of the interaction of certain HCMV proteins, indicated 5 primary pathways: IE72, IE86, and UL38 regulating mTOR; gB regulating P13K; gB/gH, UL76, UL144, and UL86 NF- κ B; IE86 and IE72 RAS/RAF/MEK1/2; and US2, US11, pp71, and UL38 UPR/proteasome degradation. In this study, we report massive profiling at the molecular pathway level of over 2,000 gene products and 600

Table 2. Changes in induction of the signaling pathways associated with the early stage of HCMV infection for HS and LS cells. Pathway activation strengths were calculated based on mRNA and miR expression data. "+" / "-" / "un" means upregulated/downregulated/unchanged state of a pathway, accordingly. Numbers indicate number of respectively regulated pathways, percentage over total pool of pathways is given in parentheses.

CMV status	mRNA+miR+	mRNA+ miR-	mRNA+ miRun	mRNA-miR+	mRNA-miR-	mRNA-miRun	mRNAun miR+	mRNAun miR-	mRNAun miRun
HS	73(29,3)	26(10,4)	4(1,6)	54(21,7)	14(5,6)	7(2,8)	32(12,8)	30(12)	9(3,6)
LS	12(5,2)	33(14,3)	13(5,6)	10(2,3)	7(3)	7(3)	58(25,2)	29(12,6)	61(26,5)

different miR molecules at the early stage of HCMV infection. Even 3 hours after infection, when viral miR molecules show little activity and viral DNA is not replicated,³⁴ we detect reshaping of expression for hundreds of cellular genes and numerous molecular pathways (Supplementary data set 4). These pathways may correspond to downstream effects of developing pathology and may contribute to a better understanding of molecular grounds of differences in sensitivity to the HCMV infection between the HS and LS cells. The HS cells showed markedly greater numbers of altered molecular pathways than the LS cells at both the PAS and the miPAS levels. It should be noted that in the earliest stages (3 hours after infection), the proportion of upregulated mRNAs was higher than of downregulated mRNAs, but according to Browne et al.,³² at the later infection stage (at 8 h after infection), the number of upregulated mRNAs, in turn, was significantly smaller than the number of downregulated mRNAs.

At least partly, the observed differences between the infected and non-infected cells may be linked with the activity of about 20 miRs encoded in the HCMV genome.³⁵⁻³⁶ However, previous findings indicate that the expression of viral miRs is hardly detectable during the first few hours of infection. For example, in lytic infection, the activity of viral miRs increases only after 24 hours and reaches maximum levels of expression after 72 hours.³⁴ To date, little is known about the interplay of cellular miRs in the early stages of HCMV infection. According to the previously published data, for the 318 miRs selected by the authors, significant changes in lytic infection occurred only 24–72 hours after exposure to HCMV. A cluster of 3 cellular microRNAs (miR-182/-96/-183) with elevated expression in HCMV-infected cells was also observed in actively proliferating tumor cells.³⁷ Here, these miR molecules weren't present in any significant amounts and have not shown significant change in expression (Supplementary data set 6). In turn, the previously

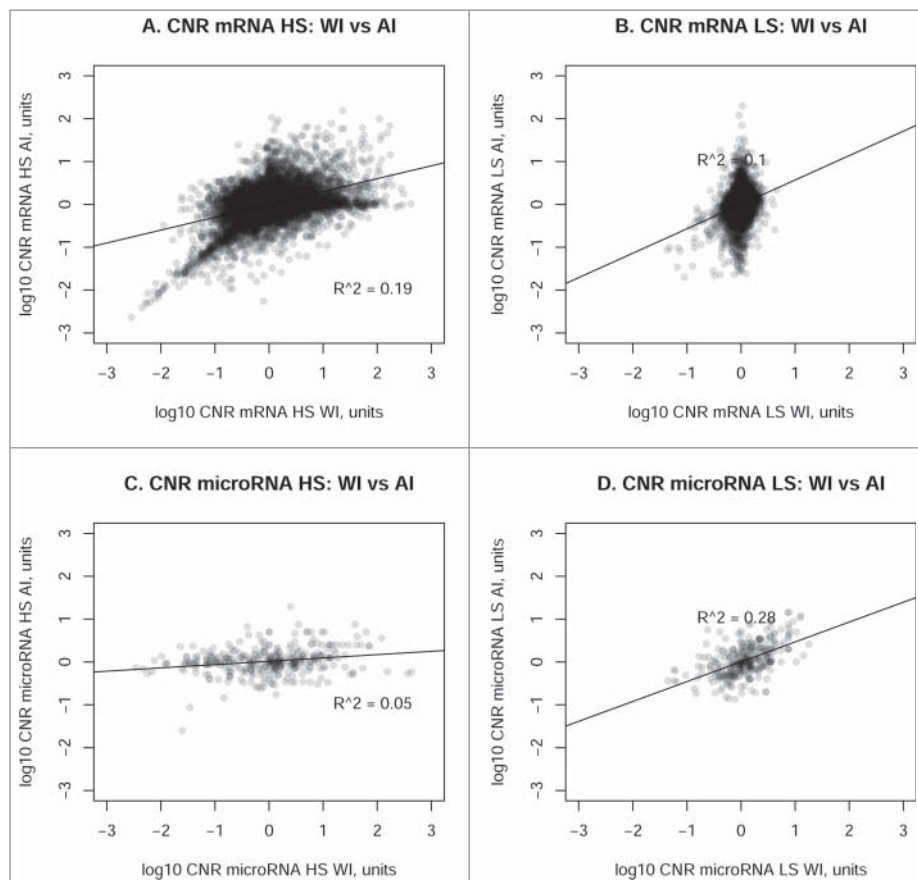


Figure 6. Dependencies between case-to-normal ratios (CNR) calculated for highly sensitive (HS) and low sensitive (LS) cells for the 3 hours after infection (AI) and 3 hours without infection (WI) conditions. Each CNR value reflects fold-change expression of a gene or an individual microRNA. Logarithms of CNR values are compared for mRNA (panels A, B) and microRNA (panels C, D) expression levels, for the AI and WI conditions. A, mRNA-based CNR data calculated for the HS cells. B, mRNA-based CNR data calculated for the LS cells. C, miR-based CNR data calculated for the HS cells. D, miR-based CNR data calculated for the LS cells.

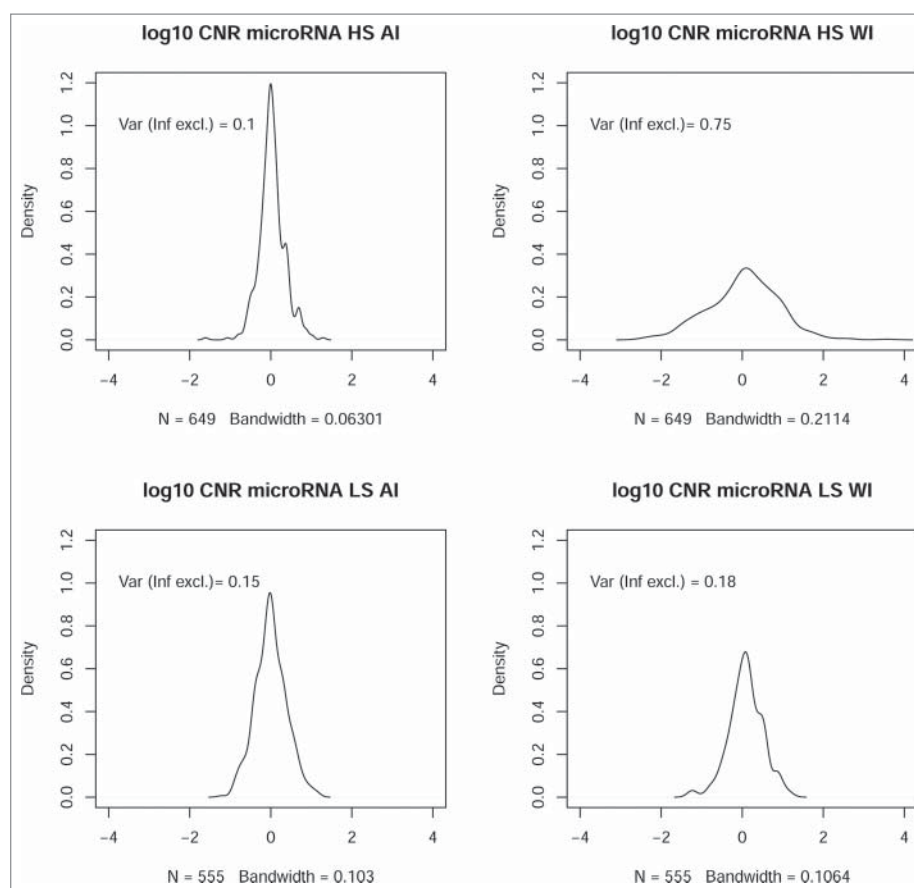


Figure 7. Distribution features of microRNA expression reflected by case-to-normal ratio (CNR), in the HS and the LS cells. The expression profiles were measured for the HCMV-infected (AI) and mock-infected (WI) cells. Abscise axis denotes logarithms of the case-to-normal ratio (CNR) values, “Density” axis – densities of the distribution. N indicates the number of individual microRNAs measured. N is different in the HS and the LS cells because of various numbers of microRNAs with zero expression levels in the respective norms. Bandwidth indicates dispersion.

published analysis of latently infected cells identified a family of cellular miRs (miR-200 family) regulating the expression of super-early, or immediately early, viral protein IE 2 and causing its repression while hindering the development of infection.³⁸ In this study, in the LS culture, there was no significant difference for these miR expression, but in the HS culture, miR-200a, miR-200b, and miR-200c were strongly downregulated in infected cells compared to mock-treated cells (Supplementary data set 6).

Here, we showed that the HCMV-infected human fibroblasts tend to form much tighter profiles of signaling pathway activation at the microRNA level, narrowly clustering around zero compared to the time-control non-infected cells (Figs. 4, 6 and 7). Overall, we observed greater levels of perturbation in the pathway activity for the HS cells as compared to the LS cells at the levels of both mRNA and miR regulation. This may be due to overall greater cell growth and cell division rates seen for the HS cells. The three - hour changes for them might be, therefore, more intense at the levels of both RNA expression and cell physiology. Three hours after infection, we detected in the HS cells almost complete suppression of internal regulation of the host-encoded miRs (Figs. 6, 7). This may be due to the HCMV repression of the early cellular antiviral protective mechanisms, where miR regulation (such as expression of miR-200a, miR-200b, and miR-200c) plays the principal role. Since the host miR regulation appeared to be repressed in faster

than 3 hours, we presume that this might be accomplished immediately upon the infection, most probably directly by the viral proteins that penetrated the target cells. In the future, understanding of this viral miR repression machinery may help to establish new artificial systems of epigenetic reprogramming of living cells.

In this study, we identified many deregulated molecular pathways associated with the early stages of HCMV infection, at both the mRNA and miR levels. The “in-depth” analysis of these features will be published elsewhere, along with the re-analyzed results of the other high-throughput studies covering early post-infectious events, such as those published by Stern-Ginossar et al.³⁹ (includes human mRNA and ribosome profiling data, but no miR data), Tirosch et al.⁴⁰ (human mRNA and ribosome profiling data, no miR data), Marcinowski et al.⁴¹ (mouse mRNA data, no miR data), Stark et al.⁴² (human mRNA and miR data, but no controls for the cells at the moment of HCMV infection).

Interestingly, it is known that in the HCMV-infected cells, polyribosome formation is stimulated and host mRNA translation proceeds uninterrupted and even at somewhat higher levels.⁴³ We speculate that the inhibition of miR metabolism discovered in this study may contribute to this paradoxical stimulation of the host mRNA translation linked with HCMV infection.

The HS cells are involved in embryonic development and the formation of the fetus, and we hope that our findings may

be used to create diagnostic tools with the potential of detecting HCMV infection at the earliest stages, even before replication of the viral genome and the manifestation of any pathological symptoms. Moreover, the application of this approach may help giving a prognosis of the severity of infection due to markedly different trends apparently seen in the HS and LS cells. Finally, the analysis of particular differential pathways identified in this study may help to elucidate molecular events guiding HCMV infection and, hopefully, to find new antiviral agents in the future.

Disclosure of potential conflicts of interest

No potential conflicts of interest were disclosed.

Funding

This work was supported by the Program of the Presidium of the Russian Academy of Sciences “Dynamics and Conservation of Genomes” and by the First Oncology Research and Advisory Center (Russia) and the Pathway Pharmaceuticals (Hong-Kong) Joint Research Initiative.

ORCID

Maxim I. Sorokin  <http://orcid.org/0000-0001-7685-3446>

Nikolay M. Borisov  <http://orcid.org/0000-0002-1671-5524>

Alla A. Kushch  <http://orcid.org/0000-0002-3396-5533>

References

- Legendre C, Pascual M. Improving outcomes for solid-organ transplant recipients at risk from cytomegalovirus infection: late-onset disease and indirect consequences. *Clin Infect Dis* 2008; 46:732-40; PMID:18220478; <http://dx.doi.org/10.1086/527397>
- Cheeran MC, Lokensgard JR, Schleiss MR. Neuropathogenesis of congenital cytomegalovirus infection: disease mechanisms and prospects for intervention. *Clin Microbiol Rev* 2009; 22:99-126; PMID:19136436; <http://dx.doi.org/10.1128/CMR.00023-08>
- Britt WJ. Vaccines against human cytomegalovirus: time to test. *Trends Microbiol* 1996; 4:34-38; PMID:8824793; [http://dx.doi.org/10.1016/0966-842X\(96\)81503-4](http://dx.doi.org/10.1016/0966-842X(96)81503-4)
- Price RL, Chiocca EA. Modeling cytomegalovirus infection in mouse tumor models. *Front Oncol* 2015; 5:61; PMID:25853089; <http://dx.doi.org/10.3389/fonc.2015.00061>
- Torres L, Tang Q. Immediate-Early (IE) gene regulation of cytomegalovirus: IE1- and pp71-mediated viral strategies against cellular defenses. *Virology* 2014; 29:343-52; PMID:25501994; <http://dx.doi.org/10.1007/s12250-014-3532-9>
- Wathen MW, Stinski MF. Temporal patterns of human cytomegalovirus transcription: mapping the viral RNAs synthesized at immediate early, early, and late times after infection. *J Virol* 1982; 41:462-77; PMID:6281461
- Weekes MP, Tomasec P, Huttlin EL, Fielding CA, Nusinow D, Stanton RJ, Wang EC, Aicheler R, Murrell I, Wilkinson GW, et al. Quantitative temporal viromics: an approach to investigate host-pathogen interaction. *Cell* 2014; 157:1460-72; PMID:24906157; <http://dx.doi.org/10.1016/j.cell.2014.04.028>
- Sorel O, Dewals BG. MicroRNAs in large herpesvirus DNA genomes: recent advances. *Biomol. Concepts* 2016; 7:229-39
- Chen X, Fan S, Song E. Noncoding RNAs: New Players in Cancers. *Adv. Exp. Med. Biol.* 2016; 927:1-47; http://dx.doi.org/10.1007/978-981-10-1498-7_1
- van Rooij E, Sutherland LB, Qi X, Richardson JA, Hill J, Olson EN. Control of stress-dependent cardiac growth and gene expression by a microRNA. *Science* 2007; 316:575-9; PMID:17379774; <http://dx.doi.org/10.1126/science.1139089>
- Xiao C, Calado DP, Galler G, Thai TH, Patterson HC, Wang J, Rajewsky N, Bender TP, Rajewsky K. MiR-150 controls B cell differentiation by targeting the transcription factor c-Myb. *Cell* 2007; 131:146-59; PMID:17923094; <http://dx.doi.org/10.1016/j.cell.2007.07.021>
- Calin GA, Ferracin M, Cimmino A, di Leva G, Shimizu M, Wojcik SE, Iorio MV, Visone R, Sever NI, Fabbri M, et al. A MicroRNA signature associated with prognosis and progression in chronic lymphocytic leukemia. *N Engl J Med* 2005; 353:533; <http://dx.doi.org/10.1056/NEJMoa050995>
- Zabolotneva A, Tkachev V, Filatov F, Buzdin A. How many antiviral small interfering RNAs may be encoded by the mammalian genomes? *Biol Direct* 2010; 5:62; PMID:21059241; <http://dx.doi.org/10.1186/1745-6150-5-62>
- Buzdin AA, Zhavoronkov AA, Korzinkin MB, Venkova LS, Zenin AA, Smirnov PY, Borisov NM. Oncofinder, a new method for the analysis of intracellular signaling pathway activation using transcriptomic data. *Front Genet* 2014; 5:55; PMID:24723936; <http://dx.doi.org/10.3389/fgene.2014.00055>
- Buzdin AA, Zhavoronkov AA, Korzinkin MB, Roumiantsev SA, Aliper AM, Venkova LS, Smirnov PY, Borisov NM. The OncoFinder algorithm for minimizing the errors introduced by the high-throughput methods of transcriptome analysis. *Front Mol Biosci* 2014; 1:8; PMID:25988149; <http://dx.doi.org/10.3389/fmolb.2014.00008>
- Makarev E, Fortney K, Litovchenko M, Braunewell KH, Zhavoronkov A, Atala A. Quantifying signalling pathway activation to monitor the quality of induced pluripotent stem cells. *Oncotarget* 2015; 6:23204-012; PMID:26327604; <http://dx.doi.org/10.18632/oncotarget.4673>
- Alexandrova E, Nassa G, Corleone G, Buzdin A, Aliper AM, Terekhanova N, Shepelin D, Zhavoronkov A, Tamm M, Milanese L, et al. Large-scale profiling of signalling pathways reveals an asthma specific signature in bronchial smooth muscle cells. *Oncotarget* 2016; 7:25150-25161; PMID:26863634; <http://dx.doi.org/10.18632/oncotarget.7209>
- Spirin PV, Lebedev TD, Orlova NN, Gornostaeva AS, Prokofjeva MM, Nikitenko NA, Dmitriev SE, Buzdin AA, Borisov NM, Aliper AM, et al. Silencing AML1-ETO gene expression leads to simultaneous activation of both pro-apoptotic and proliferation signaling. *Leukemia* 2014; 28:2222-8; PMID:24727677; <http://dx.doi.org/10.1038/leu.2014.130>
- Lezhnina K, Kovalchuk O, Zhavoronkov AA, Korzinkin MB, Zabolotneva AA, Shegay PV, Sokov DG, Gaifullin NM, Rusakov IG, Aliper AM, et al. Novel robust biomarkers for human bladder cancer based on activation of intracellular signalling pathways. *Oncotarget* 2014; 5:9022-32; PMID:25296972; <http://dx.doi.org/10.18632/oncotarget.2493>
- Aliper AM, Frieden-Korovkina VP, Buzdin A, Roumiantsev SA, Zhavoronkov A. Interactome analysis of myeloid-derived suppressor cells in murine models of colon and breast cancer. *Oncotarget* 2014; 5:11345-53; PMID:25294811; <http://dx.doi.org/10.18632/oncotarget.2489>
- Aliper AM, Csoka AB, Buzdin A, Jetka T, Roumiantsev S, Moskalev A, Zhavoronkov A. Signaling pathway activation drift during aging: Hutchinson-Gilford Progeria Syndrome fibroblasts are comparable to normal middle-age and old-age cells. *Aging (Albany NY)* 2015; 7:26-37; PMID:25587796; <http://dx.doi.org/10.18632/aging.100717>
- Makarev E, Cantor C, Zhavoronkov A, Buzdin A, Aliper A, Csoka AB. Pathway activation profiling reveals new insights into age-related macular degeneration and provides avenues for therapeutic interventions. *Aging (Albany NY)* 2014; 6:1064-75; PMID:25543336; <http://dx.doi.org/10.18632/aging.100711>
- Artibasova AV, Korzinkin MB, Sorokin MI, Shegay PV, Zhavoronkov AA, Gaifullin N, Alekseev BY, Vorobyev NV, Kuzmin DV, Kaprin AD, et al. MiRImpact, a new bioinformatic method using complete microRNA expression profiles to assess their overall influence on the activity of intracellular molecular pathways. *Cell Cycle* 2016; 15:689-98; PMID:27027999; <http://dx.doi.org/10.1080/15384101.2016.1147633>
- Brennecke J, Aravin AA, Stark A, Dus M, Kellis M, Sachidanandam R, Hannon GJ. Discrete small RNA-generating loci as master regulators of transposon activity in *Drosophila*. *Cell* 2007; 128:1089-103; PMID:17346786; <http://dx.doi.org/10.1016/j.cell.2007.01.043>
- Zabolotneva AA, Zhavoronkov AA, Shegay PV, Gaifullin NM, Alekseev BY, Roumiantsev SA, Garazha AV, Kovalchuk O, Aravin

- A, Buzdin AA. A systematic experimental evaluation of microRNA markers of human bladder cancer. *Front Genet* 2013; 4:247; PMID:24298280; <http://dx.doi.org/10.3389/fgene.2013.00247>
- [26] Langmead B, Trapnell C, Pop M, Salzberg SL. Ultrafast and memory-efficient alignment of short DNA sequences to the human genome. *Genome Biol* 2009; 10:R25; PMID:19261174; <http://dx.doi.org/10.1186/gb-2009-10-3-r25>
- [27] Li H, Handsaker B, Wysoker A, Fennell T, Ruan J, Homer N, Marth G, Abecasis G, Durbin R. 1000 Genome Project Data Processing Subgroup. The Sequence Alignment/Map format and SAMtools. *Bioinformatics* 2009; 25:2078-9; PMID:19505943; <http://dx.doi.org/10.1093/bioinformatics/btp352>
- [28] Hsu SD, Tseng YT, Shrestha S, Lin YL, Khaleel A, Chou CH, Chu CF, Huang HY, Lin CM, Ho SY, et al. miRTarBase update 2014: an information resource for experimentally validated miRNA-target interactions. *Nucleic Acids Res* 2014; 42:D78-85; PMID:24304892; <http://dx.doi.org/10.1093/nar/gkt1266>
- [29] Vlachos IS, Kostoulas N, Vergoulis T, Georgakilas G, Reczko M, Maragkakis M, Paraskevopoulou MD, Prionidis K, Dalamagas T, Hatzigeorgiou AG. DIANA miRPath v.2.0: investigating the combinatorial effect of microRNAs in pathways. *Nucleic Acids Res* 2012; 40:W498-504; PMID:22649059; <http://dx.doi.org/10.1093/nar/gks494>
- [30] Jean Beltran PM, Cristea IM. The life cycle and pathogenesis of human cytomegalovirus infection: lessons from proteomics. *Expert Rev Proteomics* 2014; 11:697-711; PMID:25327590; <http://dx.doi.org/10.1586/14789450.2014.971116>
- [31] Vergoulis T, Vlachos IS, Alexiou P, Georgakilas G, Maragkakis M, Reczko M, Gerangelos S, Koziris N, Dalamagas T, Hatzigeorgiou AG. TarBase 6.0: capturing the exponential growth of miRNA targets with experimental support. *Nucleic Acids Res* 2012; 40:D222-9; PMID:22135297; <http://dx.doi.org/10.1093/nar/gkr1161>
- [32] Browne EP, Wing B, Coleman D, Shenk T. Altered cellular mRNA levels in human cytomegalovirus-infected fibroblasts: viral block to the accumulation of antiviral mRNAs. *J Virol* 2001; 75:12319-30; PMID:11711622; <http://dx.doi.org/10.1128/JVI.75.24.12319-12330.2001>
- [33] Roy S, Arav-Boger R. New cell-signaling pathways for controlling cytomegalovirus replication. *Am J Transplant* 2014; 14:1249-58; PMID:24839861; <http://dx.doi.org/10.1111/ajt.12725>
- [34] Stark TJ, Arnold JD, Spector DH, Yeo GW. High-resolution profiling and analysis of viral and host small RNAs during human cytomegalovirus infection. *J Virol* 2012; 86:226-35; PMID:22013051; <http://dx.doi.org/10.1128/JVI.05903-11>
- [35] Landais I, Pelton C, Streblow D, de Filippis V, McWeeney S, Nelson JA. Human Cytomegalovirus miR-UL112-3p Targets TLR2 and Modulates the TLR2/IRAK1/NFκB Signaling Pathway. *PLoS Pathog* 2015; 11:e1004881; PMID:25955717; <http://dx.doi.org/10.1371/journal.ppat.1004881>
- [36] Li C, Hu J, Hao J, Zhao B, Wu B, Sun L, Peng S, Gao GF, Meng S. Competitive virus and host RNAs: the interplay of a hidden virus and host interaction. *Protein Cell* 2014; 5:348-56; PMID:24723323; <http://dx.doi.org/10.1007/s13238-014-0039-y>
- [37] Schaefer A, Jung M, Mollenkopf HJ, Wagner I, Stephan C, Jentzmik F, Miller K, Lein M, Kristiansen G, Jung K. Diagnostic and prognostic implications of microRNA profiling in prostate carcinoma. *Int J Cancer* 2010; 126:1166-76; PMID:19676045
- [38] O'Connor CM, Vanicek J, Murphy EA. Host microRNA regulation of human cytomegalovirus immediate early protein translation promotes viral latency. *J Virol* 2014; 88:5524-32; <http://dx.doi.org/10.1128/JVI.00481-14>
- [39] Stern-Ginossar N, Weisburd B, Michalski A, Le VT, Hein MY, Huang SX, Ma M, Shen B, Qian SB, Hengel H, Mann M, Ingolia NT, Weissman JS. Decoding human cytomegalovirus. *Science* 2012; 338:1088-93; PMID:23180859; <http://dx.doi.org/10.1126/science.1227919>
- [40] Tirosh O, Cohen Y, Shitrit A, Shani O, Le-Trilling VT, Trilling M, Friedlander G, Tanenbaum M, Stern-Ginossar N. The Transcription and Translation Landscapes during Human Cytomegalovirus Infection Reveal Novel Host-Pathogen Interactions. *PLoS Pathog*. 2015; 11:e1005288; PMID:26599541
- [41] Marcinowski L, Lidschreiber M, Windhager L, Rieder M, Bosse JB, Rädle B, Bonfert T, Györy I, de Graaf M, Prazeres da Costa O, Rosenstiel P, Friedel CC, Zimmer R, Ruzsics Z, Dölken L. Real-time transcriptional profiling of cellular and viral gene expression during lytic cytomegalovirus infection. *PLoS Pathog*. 2012; 8:e1002908; PMID:22969428
- [42] Stark TJ, Arnold JD, Spector DH, Yeo GW. High-resolution profiling and analysis of viral and host small RNAs during human cytomegalovirus infection. *J Virol*. 2012; 86:226-35; PMID:22013051
- [43] Stinski MF. Synthesis of proteins and glycoproteins in cells infected with human cytomegalovirus. *J Virol* 1977; 23:751-67; PMID:197270